Human Molecular Genetics, 2012, Vol. 21, No. 15 **3333–3344**
doi:10.1093/hmg/dds163
Advance Access published on April 27, 2012

OCRL localizes to the primary cilium: a new role for cilia in Lowe syndrome

Na Luo[1], Callah C. West[1], Carlos A. Murga-Zamalloa[6], Lou Sun[1], Ryan M. Anderson[2], Clark D. Wells[3], Robert N. Weinreb[5], Jeffrey B. Travers[4], Hemant Khanna[7] and Yang Sun[1,*]

[1]Department of Ophthalmology, Glick Eye Institute, [2]Department of Pediatrics, [3]Department of Biochemistry and Cell Biology and [4]Department of Dermatology, Indiana University, 1601 W Michigan St., Indianapolis, IN 46202, USA, [5]Department of Ophthalmology, University of California San Diego, San Diego, CA, USA, [6]Department of Pathology, University of Michigan Medical School, Ann Arbor, MI, USA and [7]Department of Ophthalmology, University Massachusetts Medical School, Worcester, MA, USA

Received March 18, 2012; Revised April 12, 2012; Accepted April 20, 2012

Oculocerebral renal syndrome of Lowe (OCRL or Lowe syndrome), a severe X-linked congenital disorder characterized by congenital cataracts and glaucoma, mental retardation and kidney dysfunction, is caused by mutations in the *OCRL* gene. OCRL is a phosphoinositide 5-phosphatase that interacts with small GTPases and is involved in intracellular trafficking. Despite extensive studies, it is unclear how *OCRL* mutations result in a myriad of phenotypes found in Lowe syndrome. Our results show that OCRL localizes to the primary cilium of retinal pigment epithelial cells, fibroblasts and kidney tubular cells. Lowe syndrome-associated mutations in *OCRL* result in shortened cilia and this phenotype can be rescued by the introduction of wild-type OCRL; *in vivo*, knockdown of *ocrl* in zebrafish embryos results in defective cilia formation in Kupffer vesicles and cilia-dependent phenotypes. Cumulatively, our data provide evidence for a role of OCRL in cilia maintenance and suggest the involvement of ciliary dysfunction in the manifestation of Lowe syndrome.

INTRODUCTION

Mutations in the Oculocerebrorenal syndrome (*OCRL*) gene are associated with Lowe and Dent syndromes (1–3). While both diseases exhibit renal tubular pathologies, only Lowe syndrome is associated with pleomorphic features, including bilateral congenital cataracts, glaucoma, hypotonous muscles and mental retardation (1–3). Although OCRL has been identified as an inositol polyphosphate 5-phosphatase (INPP5E), the mechanisms of disease for OCRL mutations in causing these phenotypes are unclear.

A common role of the different functional modalities of OCRL is the regulation of membrane trafficking. OCRL is reported to distribute to the trans-Golgi network (TGN), endosomes, phagosomes and specific regions of the plasma membrane at adherens and tight junction (4–12). OCRL can directly bind to several proteins that couple it to the regulation of endocytosis; for instance, OCRL binds clathrin in a manner that partially accounts for its ability to promote endocytosis (6,7,9–11,13–17). Further, a region within the c-terminal RhoGAP-like domain of OCRL, in which several disease-causing mutations are found, binds to a short phenylalanine and histidine (F&H) motif found within the endocytic adaptors APPL1 and Ses1/2 (18,19). OCRL is also linked to endosomal functions through a rab family of small GTPase (RAB)-binding domain that associates with RAB5 (7), RAB8A (7,20) and RAB35 (14), as well as to the small GTPases ARF1 and ARF6 (21). At the plasma membrane, OCRL inhibits membrane ruffling and actin polymerization by limiting the levels of phosphatidylinositol-4, 5-bisphosphate (PIP_2) (22,23).

Similarities between OCRL and another INPP5E suggest that OCRL might also function in cilia. Primary cilia are conserved eukaryotic structures that protrude from the cell surface to detect and transduce environmental cues in nearly all mammalian cells (24–32). Non-motile sensory cilia consist of an array of bundled microtubules (axoneme) that are

*To whom correspondence should be addressed. Tel: +1 3172781878; Fax: +1 3172747744; Email: sunyo@iupui.edu

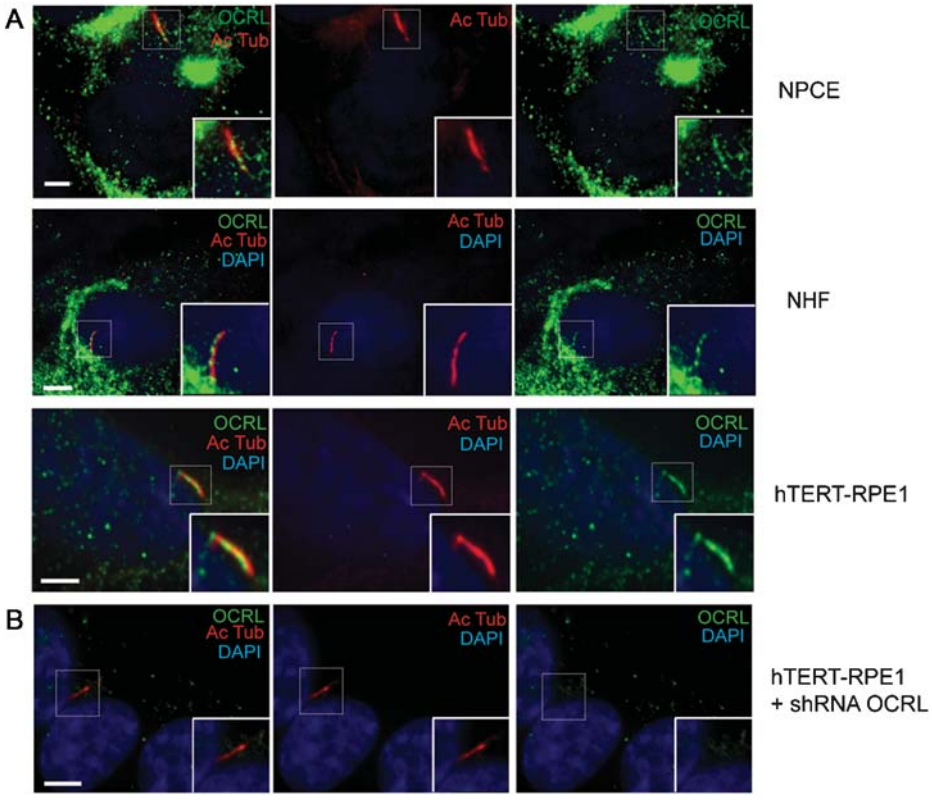

Figure 1. OCRL localize to primary cilia in ocular and renal cells. (**A**) Immunofluorescence of NPCE cells, NHF and hTERT-RPE1 serum starved for 48 h was performed using rabbit anti-OCRL antibody (green), mouse anti-acetylated α-tubulin antibody (red) and DAPI (blue). Insert shows OCRL colocalization with acetylated α-tubulin. Scale bar 5 μm. (**B**) OCRL knockdown hTERT-RPE1 cells were serum starved for 24 h and immunostained with anti-acetylated α-tubulin (red) and OCRL (green) antibodies (DAPI, blue). Scale bar 5 μm.

covered by a plasma membrane enriched in cholesterol and monophosphorylated phosphatidylinositols (33,34). Axonemal microtubules arise from a specialized microtubule nucleating center termed the basal body (32,34–37). Defects in the formation of the primary cilium result in several clinical features collectively referred to as ciliopathies (38–40). INPP5E, which catalyzes the removal of phosphate from the 5-position on inositol polyphosphates similar to OCRL (41), localizes to primary cilium of both renal tubular cells and retinal pigment epithelial cells (42). Mutations in INPP5E result in ciliary instability and are associated with Joubert syndrome (42).

Because of the emerging role of phosphoinositides in primary cilium function, we investigated the role for OCRL in regulating this structure. We found that OCRL localizes to the primary cilium. Further, perturbation of OCRL results in ciliary defects in both cultured cells and developing zebrafish. A new role for OCRL in primary cilia formation is therefore proposed that may explain why mutants of OCRL contribute to the pathogenesis of Lowe syndrome.

RESULTS

OCRL localizes to the cilia and the basal body in ocular and renal tissues

While mutations in *OCRL* are associated with a wide spectrum of phenotypes in Lowe syndrome patients (43), the localization of OCRL in the affected cells is not well characterized. We sought to examine the ocular cells that develop cilia such as non-pigment ciliary epithelial (NPCE) (44). We used a previously described OCRL antibody and confirmed its specificity (6); in the presence of a blocking peptide, OCRL signal is undetectable by immunoblotting or by immunofluorescence (Supplementary Material, Fig. S1A and B). In addition, the immunoreactive band is absent in two established fibroblast cell lines derived from Lowe patients (Lowe 1676 and 3265) and decreased in fibroblast cells transfected with *OCRL* siRNA (Supplementary Material, Fig. S1C). In cultured NPCE cells that have been serum starved for 48 h, OCRL localization was examined by immunofluorescence, which showed immunostaining of OCRL in the primary cilium, as determined by co-staining with a monoclonal antibody against acetylated α-tubulin (Ac Tub), a marker for cilia (45) (Fig. 1A). In addition, OCRL was distributed in the cilium with acetylated α-tubulin of serum-starved normal human fibroblast (NHF) and hTERT-RPE1 cells, both ciliated cell types (46,47) (Fig. 1A). Also in serum-starved hTERT-RPE1 cells, endogenous OCRL was seen to colocalize to γ-tubulin, a basal body marker (Supplementary Material, Fig. S1D). After 48 h of serum starvation, OCRL was mainly detected ($>60\%$) within the basal body of hTERT-RPE cells and only slightly ($< 10\%$) in the ciliary axoneme (Supplementary Material, Fig. S1E).

Staining for OCRL is specific as it is ablated by preincubation of the OCRL antibody with an OCRL-specific peptide epitope (Supplementary Material, Fig. S1B).

Furthermore, no OCRL staining was detected in hTERT-RPE1 cells that have stable silencing of OCRL expression by shRNA with lentiviral transduction (Fig. 1B). Additionally, OCRL was found in the cilia by other methods: enhanced green fluorescent protein (EGFP)-tagged OCRL was detected in the cilia of stably transfected hTERT-RPE cells after 24 h serum starvation (Supplementary Material, Fig. S2A); Flag-tagged OCRL was found in the cilia NHF cells that were serum starved for 24 h and stained for acetylated α-tubulin (Supplementary Material, Fig. S2B). Finally, endogenous OCRL was also detected in the cilium of 24 h serum-starved NHF with an entirely different OCRL antibody, which is a monoclonal (ms) antibody (Supplementary Material, Fig. S2C and D).

In addition to subcellular localization in cultured cells, OCRL expression in human tissues was determined. Initially, cross-sections from human eyes were immunostained with the previous characterized antibody against OCRL. This revealed that OCRL is expressed in the retina and the retinal pigment epithelium (RPE) (Supplementary Material, Fig. S2E). Further analysis revealed that OCRL localizes to the photoreceptor outer segment, which is an extension of the specialized photoreceptor sensory cilium (Supplementary Material, Fig. S2E). As renal disease is observed in Lowe syndrome, OCRL localization was also examined in rat kidney sections. Immunostaining of OCRL was detected along the primary cilium of kidney tubular cells that were marked by co-staining with antibodies against the acetylated α-tubulin (Supplementary Material, Fig. S2F). Taken together, OCRL is shown to partition to the basal body and axoneme of primary cilium in ocular-ciliated cell lines, retinal tissue, kidney tubular cells and fibroblasts.

OCRL recruitment to cilia is modulated by RAB8A

Since OCRL was detected in the cilia, the temporal dynamics whereby OCRL distributes to cilia was examined. OCRL localization was evaluated in hTERT-RPE1 cell lines after serum starvation for different time points. OCRL predominantly localizes at the primary cilium at an early time point, within 20 min of serum starvation (Fig. 2A), as well at 50 and 90 min (data not shown). Recent structural studies showed that OCRL tightly binds to RAB8A (20), a small GTPase required for targeting multiple proteins to the primary cilium (47,48). RAB8A has been demonstrated to enter cilia during early ciliogenesis (49). Therefore, we hypothesized that OCRL may be recruited in early ciliogenesis with RAB8A. When bound to GDP, RAB8A is located in the cytosol, whereas GTP-bound RAB8A distributes to the primary cilium in serum-starved cells (50). Thus, the co-localization of transiently expressed GFP-tagged RAB8A [wild-type (WT)] or RAB8A (T22N) (GDP-bound) with endogenous OCRL was examined. This revealed that OCRL co-localizes with GFP-tagged RAB8A (WT) (70%) at the primary cilium, but not with the GDP-locked RAB8A (T22N) (19%) (Fig. 2B and C); thus, overexpression of RAB8A (WT) increased the degree of OCRL localization to the cilia.

The impact of silencing the expression of RAB8A on OCRL accumulation in the primary cilium of hTERT-RPE1 cells was also determined. Approximately 50% of the cells expressing an shRNA-targeting RAB8A (Supplementary Material, Fig. S3A) had undetectable levels of OCRL at the primary cilium when compared with the 80% of the cells expressing a scramble control showed OCRL staining with γ-tubulin (Fig. 2D and E). To elucidate the requirement of RAB8A binding to OCRL for its targeting to the primary cilium, the localization of a mutant of OCRL (F668V), which abolishes the interaction with RAB8A (20), was investigated in hTERT-RPE1 cells. As shown in Figure 2F, OCRL (F668V) was undetectable in cilia of hTERT-PRE1 cells serum starved for 48 h.

Enzymatic domain of OCRL regulates its localization at the primary cilium

To assess the function of OCRL in primary cilia, we generated hTERT-RPE1 cells stably expressing OCRL-shRNA and control (scrambled) shRNA. hTERT-RPE1 cells with OCRL knockdown (Fig. 3A) showed a marked reduction in cells with detectable cilia when compared with control cells at both 24 and 42 h following serum starvation (Fig. 3B). In addition, OCRL knockdown cells with cilia showed a 20% reduction in cilia length versus control cells (Fig. 3C) at 24 h (4.1 versus 3.2 μm, respectively) and 42 h (4.5 versus 3.4 μm, respectively).

Lowe patients frequently present with mutations of OCRL in the 5-phosphatase domain or in the RhoGAP domain (5,51). To better understand the effects of such mutations, human disease-associated mutants of *OCRL*, D499A and D422A (Fig. 3D) in the phosphatase domain as well as a deletion mutant of OCRL that lacks its RhoGAP domain (DeltaRhoGAP) were examined for their localization at the primary cilium. Flag-tagged *OCRL* WT, *OCRL* (D499A), *OCRL* (D422A) or GFP-tagged *OCRL* (DeltaRhoGAP) were transfected into ciliated RPE cells. Immunofluorescence analysis in Figure 3E showed that although WT OCRL was detected at cilia, neither of the OCRL D499A or D422A mutants was visible at cilia. The EGFP-tagged *OCRL*-DeltaRhoGAP localized near the base but not along the length of the cilia (Fig. 3E). Ciliary length analysis in Figure 3F showed that the cells expressing phosphatase-dead mutants of OCRL exhibited shorter cilia when compared with OCRL WT. In addition, the RhoGAP deletion mutant resulted in the shortened cilia length. We then tested the ability of these mutant proteins to interact with RAB8A. For this purpose, Flag-tagged *OCRL* (WT), *OCRL* (D499A), or *OCRL* (D422A), *OCRL* (F668V), or *OCRL* (Delta-RhoGAP) were transiently co-transfected into HEK-293 cells with *GFP-RAB8A*. We observed relatively similar levels of co-immunoprecipitation of Rab8A with all OCRL forms except the F668V mutant, which has impaired Rab8A interaction (Supplementary Material, Fig. S3B and C).

Primary cilia defect in Lowe patient fibroblasts

We next evaluated the relationship between OCRL and the integrity of primary cilium in the two Lowe patient fibroblast cell lines (Lowe 1676 and 3265). First, the length of the primary cilium was evaluated following serum starvation for 24 h. Both Lowe fibroblast cell lines exhibited ∼30% shorter cilia than the NHF controls (Fig. 4A and B). Similar

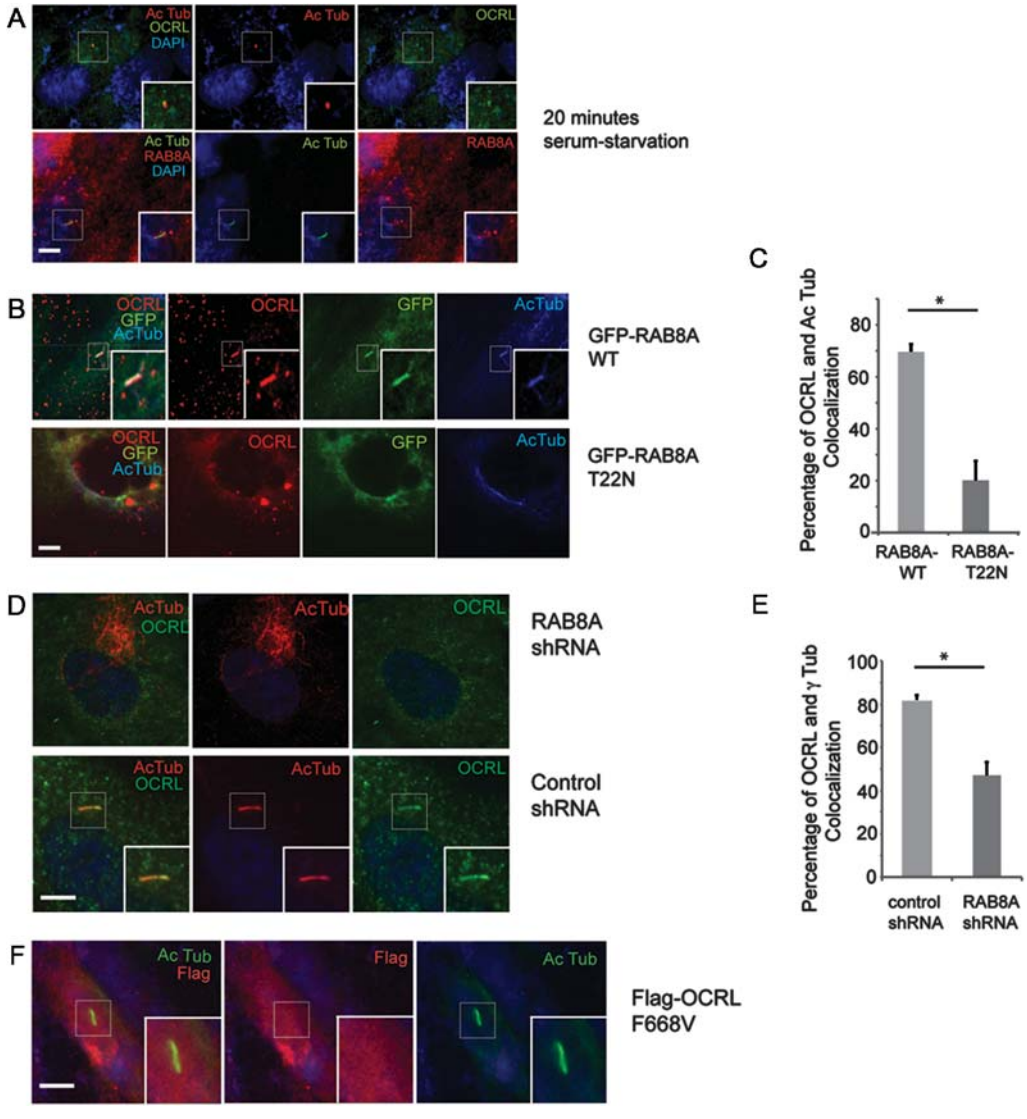

Figure 2. OCRL associates with RAB8A in primary cilia. (**A**) OCRL and RAB8A are recruited to the cilia during early ciliogenesis. hTERT-RPE1 cells were serum starved for 20 min, and immunofluorescence was performed using rabbit anti-OCRL antibody (green), mouse anti-acetylated α-tubulin antibody (red) and DAPI (blue). In a parallel experiment, immunofluorescence was performed with mouse anti-RAB8A antibody (red), rabbit anti-acetylated α-tubulin antibody (green) and DAPI (blue). (**B**) GFP-RAB8A (WT) and GFP-RAB8A (T22N) were transfected into hTERT-RPE1 cells for 48 h, then cells were serum starved for 24 h and immunofluorescence was done using rabbit anti-OCRL (red) and mouse anti-acetylated α-tubulin (blue) antibodies. (**C**) The percentage of co-localization of OCRL and acetylated α-tubulin was determined for each group and is displayed in the graph ($^*P < 0.01$, $n = 3$, total cells counted >100 per group). (**D**) Loss of RAB8A resulted in decreased OCRL recruitment to the primary cilia. RAB8A and control stable knockdown hTERT-RPE1 cells were serum starved for 48 h and immunofluorescence was performed using rabbit anti-OCRL (green), mouse anti-acetylated α-tubulin (red) antibody and DAPI (blue). (**E**) RAB8A and control stable knockdown hTERT-RPE1 cells were serum starved for 48 h and immunofluorescence was performed using rabbit anti-OCRL and mouse anti γ-tubulin antibodies. The percentage of co-localization of OCRL and γ-tubulin was determined for each group and is displayed in the graph ($^*P < 0.01$, $n = 3$, total cells counted >100 per group). (**F**) Transfection of Flag-OCRL (F668V) into hTERT-RPE1 cells for 48 h, followed by serum starvation for 24 h and immunostaining using mouse anti-Flag antibody (red), rabbit anti-acetylated α-tubulin antibody (green) and DAPI (blue). Scale bar 5 μm.

findings were observed under 48 h serum starvation (data not shown). While serum starvation induces ciliogenesis, serum stimulation leads to the cilia disassembly, allowing the cells to exit quiescence and re-enter the cell cycle (42). Cilia disassembly was evaluated by measuring cilia length 4 h following serum stimulation (Fig. 4B). In this case, cilia length decreased from 4.4 to 2.7 μm in NHF, whereas the cilia length of the Lowe patient fibroblasts retracted from 2.8 to 1.4 μm in the 1676 mutant and from 2.8 to 1.7 μm in the 3265 mutant.

We then assessed whether the expression of WT OCRL can rescue the ciliary defects in patient fibroblasts. Flag-OCRL was observed to localize with acetylated α-tubulin at the primary cilium of transfected Lowe fibroblasts (Supplementary Material, Fig. S4A). Upon serum starvation for 24 h, Lowe patient fibroblasts with transfected WT OCRL developed cilia with similar lengths as NHF controls (Fig. 4B, Supplementary Material, Fig. S4B). However, the expression of OCRL (F668V) did not rescue cilia defects in these cells (Supplementary Material, Fig. S4C). Taken together, Lowe

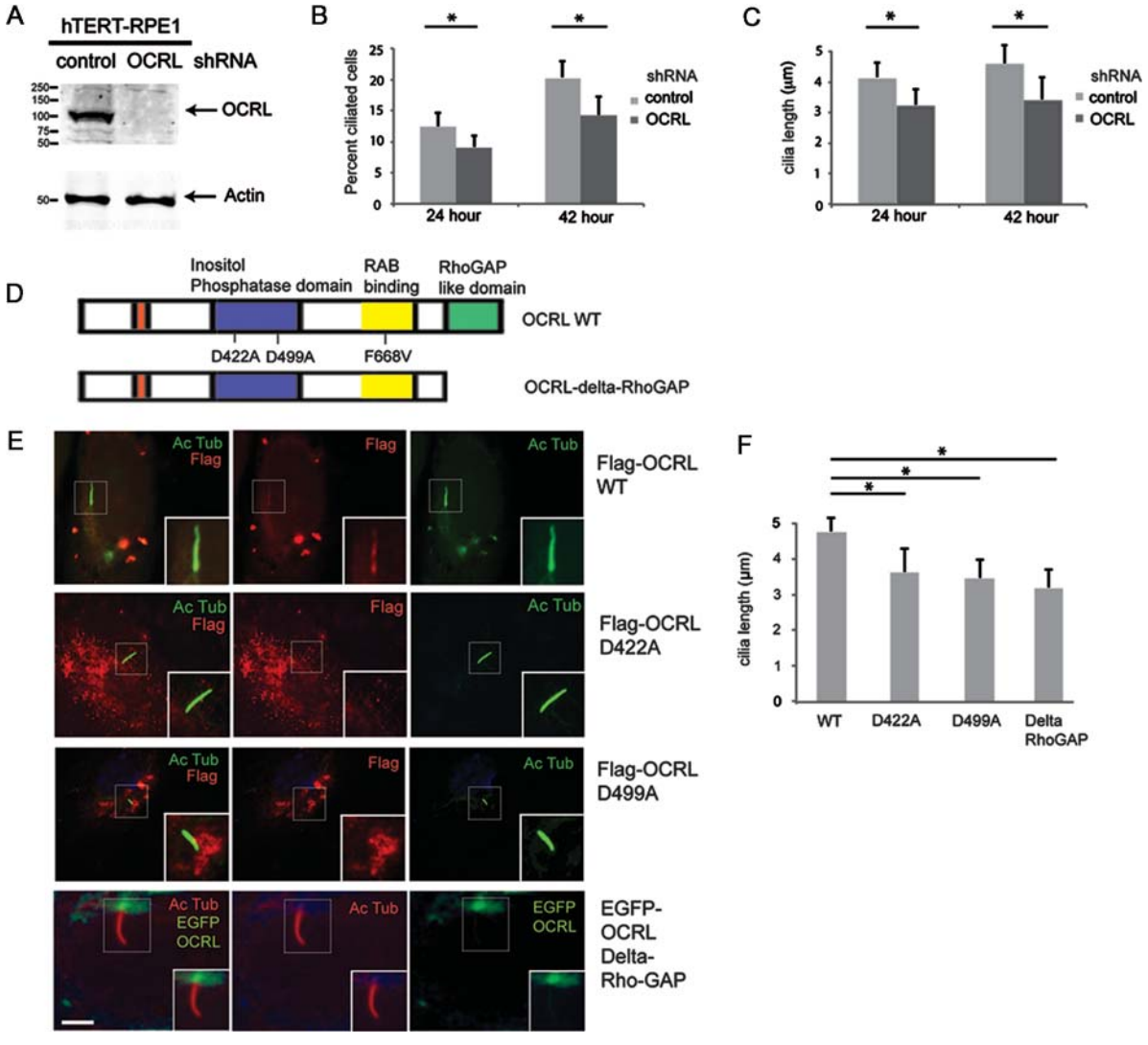

Figure 3. OCRL mutants fail to localize to the cilia. (**A**) Stable knockdown cell lines of OCRL and control shRNA were generated in hTERT-RPE1 cells. Forty microgram of total protein was separated by sodium dodecyl sulfate–polyacrylamide gel electrophoresis followed by immunoblot analysis using rabbit anti-OCRL and mouse anti-actin antibodies. (**B**) OCRL knockdown cells exhibit decreased cilia formation. Control and OCRL stable knockdown hTERT-RPE1 cells were serum starved for either 24 or 42 h, and then immunofluorescence was performed using mouse anti-acetylated α-tubulin antibody. The number of ciliated cells was then quantified ($^*P < 0.05$, $n = 3$, total cells counted >100 per group). (**C**) OCRL knockdown cells exhibit shortened cilia formation. Control and OCRL stable knockdown hTERT-RPE1 cells were serum starved for 24 or 42 h and then the immunofluorescence was performed using mouse anti-acetylated α-tubulin antibody. The length of the cilia was quantified ($^*P < 0.05$, $n = 3$, total cells counted >100 per group). (**D**) Structural domains of OCRL and generated mutants. (**E** and **F**) Transfection of Flag-OCRL (WT), Flag-OCRL (D422A), Flag-OCRL (D499A) or EGFP-OCRL (Delta-RhoGAP) into hTERT-RPE1 cells for 48 h, followed by serum starvation for 24 h and immunostaining using mouse anti-Flag antibody (red), rabbit anti-acetylated α-tubulin antibody (green) and DAPI (blue). The ciliary length was determined for each group and is displayed in the graph ($^*P < 0.05$, $n = 3$, total cells counted >50 per group). Scale bar 5 μm.

syndrome fibroblasts exhibit a ciliary defect that can be rescued by the WT OCRL.

Loss of OCRL expression in zebrafish embryos results in cilia defects

To determine the functional significance of OCRL in cilia formation during vertebrate development, *ocrl* expression was knocked down in zebrafish embryos. In all cases, the knockdown effects were confirmed with two different antisense morpholinos against *ocrl*, MO-1 and MO-2; MO-1 blocks the transcription of *ocrl* and MO-2 blocks the splicing of *ocrl* (splice junction of intron 21 and exon 22). Injection of either *ocrl* MO-1 or MO-2 resulted in reduced *ocrl* mRNA level when compared with *gapdh*; a 5 bp mismatch control MO had no effect (Supplementary Material, Fig. S5A). Following injection of *ocrl* MO1, MO2 or mismatch MO into one-cell embryos, morphant phenotypes were investigated at 48 h post-fertilization (hpf). Morphants injected with mismatch MO appeared normal, whereas those injected with *ocrl* MO-1 or MO-2 exhibited microphthalmia, body-axis asymmetry, kinked tail and hydrocephalus (Fig. 5A). Both morphants also developed ocular defects including microlentis (a smaller ocular lens) and distorted

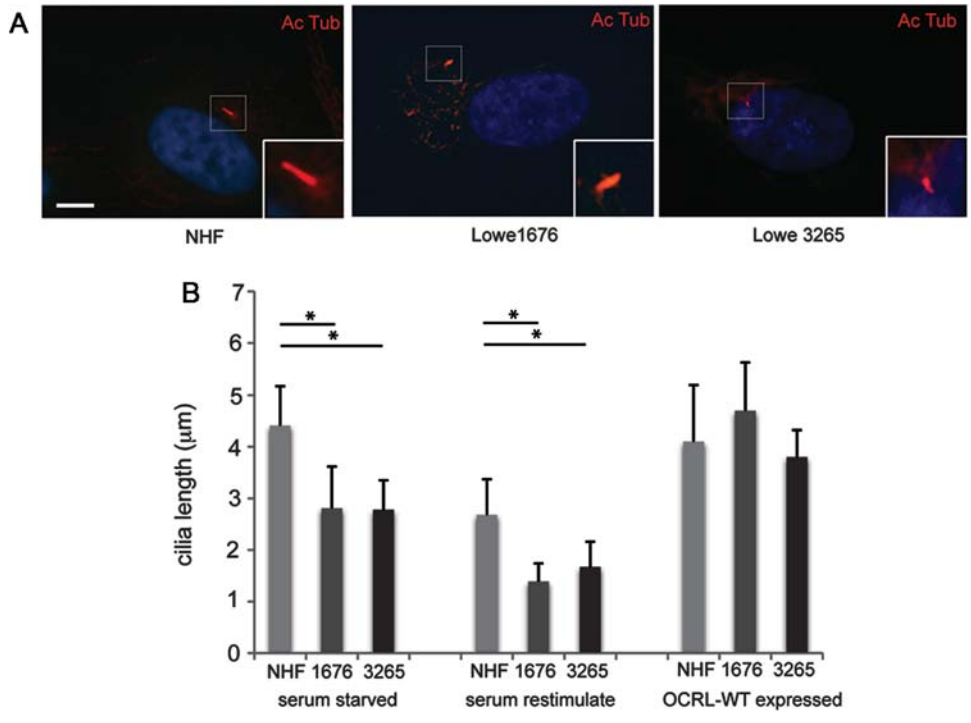

Figure 4. Primary cilia instability in Lowe fibroblasts. (**A**) Representative images of NHF, Lowe 1676 and Lowe 3265 cells that were serum starved for 24 h, re-stimulated with serum for 4 h and then stained by immunofluorescence using mouse anti-acetylated α-tubulin antibody (red). Scale bar 5 μm. (**B**) NHF, Lowe 1676 and Lowe 3265 cells were either serum starved for 24 h or serum starved for 24 h and then re-stimulated with serum for 4 h, or transduced with OCRL WT containing lentivirus and serum starved for 24 h; different treatment groups are shown in graph separately. Immunofluorescence was performed using mouse anti-acetylated α-tubulin antibody and DAPI (blue). The cilia length was measured by two different observers ($^*P < 0.01$, $n = 3$, total cells counted >100 per group, ANOVA analysis).

retinas versus control MO-injected zebrafish (Fig. 5A). These phenotypes resemble those seen in several zebrafish models of ciliopathies (52,53). Approximately 70% of *ocrl* MO-1 or MO-2 injected morphants reproducibly exhibited microphthalmia at 48 hpf (Fig. 5B). The penetrance of microphthalmia, kinked tail and body-axis asymmetry phenotypes was directly related to the dose of injected *ocrl* MO-1 (Fig. 5C) or MO-2 (data not shown). To demonstrate that the loss of *ocrl* is causal for these phenotypes, human OCRL mRNA was co-injected with *ocrl* MO-1 into zebrafish embryos. These morphants developed in a similar fashion as those injected with the mismatch MO (Fig. 5D, Supplementary Material, Fig. S5B). Thus, defects in cilia function are proposed to underlie the phenotypes observed in *ocrl* depleted morphants.

To further establish that *ocrl* is necessary for cilia formation during zebrafish development, the effect of loss of OCRL expression on Kupffer vesicle (KV) formation was investigated. The KV is a ciliated, fluid-containing structure in the zebrafish, orthologous to the mouse embryonic node; it regulates left–right body axis and organ development through directional cilia rotation (54). Cilia in the KV of morphants injected with *ocrl* MO-1 or mismatch MO was analyzed by immunohistochemistry using an antibody against acetylated α-tubulin. Compared with mismatch MO-injected morphants, *ocrl* MO-1-injected morphants displayed an approximate 40% decrease in the number and the length of cilia in the KV (Fig. 5E, Supplementary Material, Fig. S5C). Taken together, *ocrl* is concluded to function in cilia development in zebrafish.

DISCUSSION

Defects in cilia formation or maintenance have been associated with degeneration of multiple organs including the eye, brain and kidney (55–57). A spectrum of the ciliopathies range from mild to severe, including Usher Syndrome, Bardet–Biedl Syndrome, Joubert Syndrome, Leber congenital amaurosis and Merkel Syndrome (3,38,56,58–62). This study explored a novel role of inositol phosphatase and phosphoinositide signaling components in the formation and function of the primary cilium. We show that the OCRL protein, whose gene mutations cause Lowe and Dent syndromes, is localized to the primary cilia and involved in ciliary function.

Previously, OCRL has been shown to localize in a number of subcellular compartments, including the TGN and endosomes (7,13,15,63). Our study provides support that phosphoinositides play an important role in regulating the primary cilium. Using multiple approaches, we show that OCRL localizes to both the basal body and the transition zone of the primary cilium; the distribution of OCRL to the basal body and the transition zone of the primary cilia are consistent with several other ciliary proteins (64,65). Additionally, our zebrafish studies showed that *ocrl* morphants developed microphthalmia and microlentis, which has been observed in patients with Lowe syndrome (66); we hypothesize that the mechanism of observed microphthalmia may be related to a defective AKT signaling cascade seen in INPP5E-associated ciliopathies (42). INPP5E mutations in the 5-phosphatase domain are associated with Joubert and

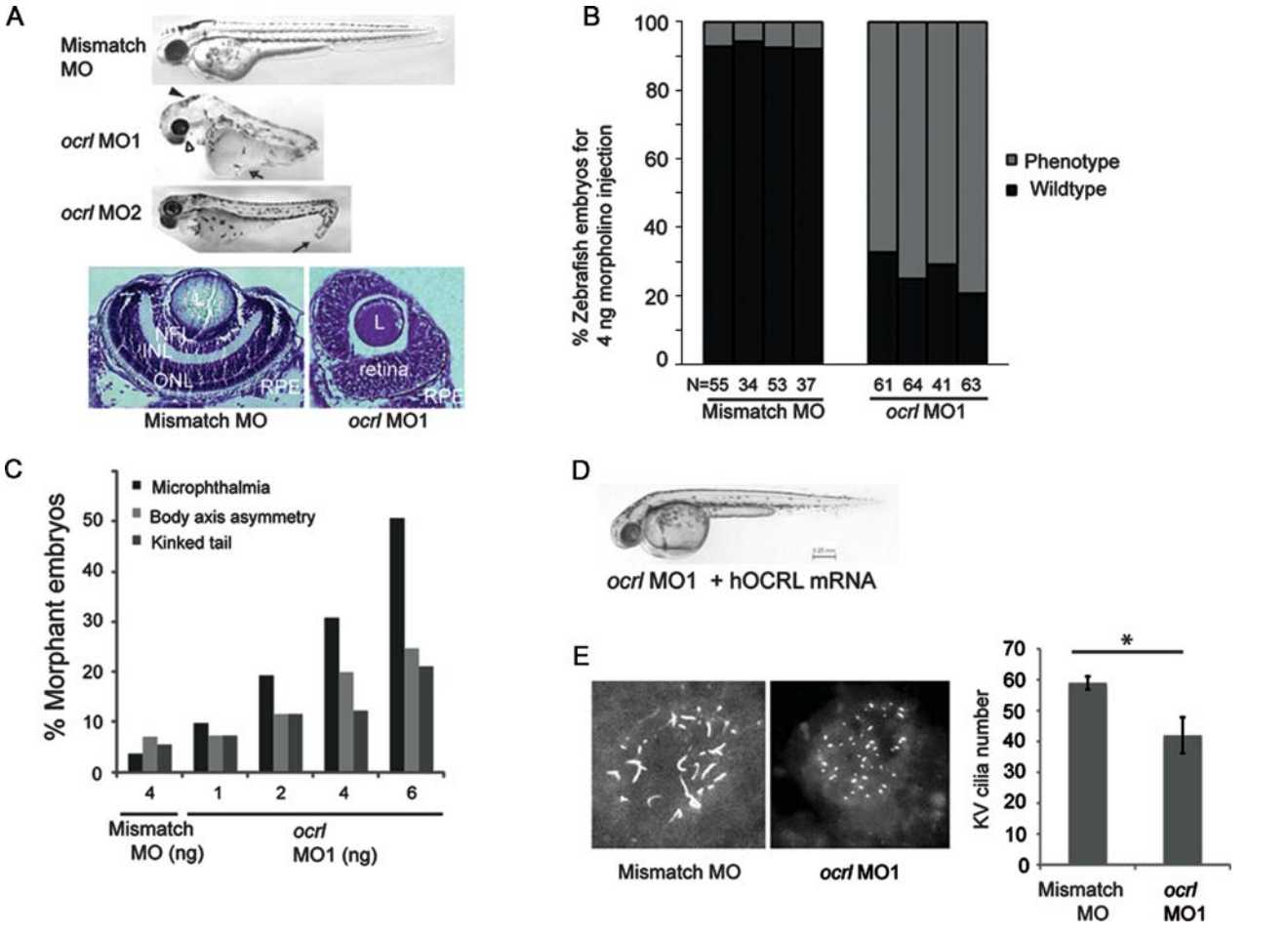

Figure 5. Zebrafish morphants of OCRL exhibit ciliary defects. (**A**) Generation of OCRL morphants. (Top panel) Zebrafish embryos were injected with mismatch control, *ocrl* MO1 or *ocrl* MO2 and phenotype assessed at 48 hpf. From lateral side photos on the top, representative phenotypes of microphthalmia (white arrowhead), hydrocephalus (solid arrowhead), body-axis asymmetry, generalized edema (white arrow), kinked tail (solid arrow) and hypopigmentation were observed in *ocrl* MO1 and MO2 morphants. (Bottom panel) Zebrafish embryos injected with control or *ocrl* MO1 were fixed at 48 hpf, ocular sections were obtained and subjected to cresyl violet staining (L, lens; NFL, nerve fiber layer; INL, inner nuclear layer; ONL, outer nuclear layer; RPE, retinal pigment epithelium). (**B**) *ocrl* MO1 (4 ng) and mismatch MO (4 ng) were injected into one-cell zebrafish embryos. By 48 hpf, all the phenotypes were assessed together against WT fish and the total numbers of defective morphants in four independent experiments were quantified. (N, the number of injected embryos). (**C**) Dose-dependent effect of morpholinos in zebrafish. Indicated doses of *ocrl* MO1 or mismatch MO were injected into zebrafish embryos and microphthalmia, kinked tail or body asymmetry were quantified. Data are representative of samples in the same injection experiments ($N > 40$). (**D**) Rescue of phenotype by WT hOCRL mRNA. Zebrafish embryos were injected with *ocrl* MO1 with hOCRL mRNA and assessed at 48 hpf. Representative image shows a zebrafish that received co-injection of *ocrl* MO1 (4 ng) and hOCRL mRNA (500 pg) ($N > 40$). (**E**) Representative images and graph show that knockdown of *ocrl* affects KV cilia formation. KV cilia were analyzed by immunofluorescence with anti- acetylated α-tubulin (red) at the six-somite stage. Quantification of number (right) of KV cilia is shown ($^*P < 0.01$, $n = 3$, total embryo >10 per group).

MORM syndromes (42,67); similarly, mutations in the 5-phosphatase domain of OCRL also result in shorten cilia, suggesting that the inositol phosphatase activity is important in cilia maintenance. In addition, we showed that the loss of the RhoGAP domain in OCRL affects its ciliary localization, which may be due to its interaction with the lipid membrane of vesicles.

RAB GTPases are important regulators of vesicular trafficking and polarity formation (47,48), and OCRL is known to interact with a number of RAB proteins through its RAB-binding domain (7,20). Interestingly, RAB8 has been recognized as a common RAB GTPase for both OCRL and INPP5B (68), and our study shows similar temporal recruitment of both OCRL and RAB8A to the primary cilia. Since RAB8A is a key regulator of cilia development, it is not surprising that the interaction between OCRL and RAB8 is important for its ciliary function.

The identification of OCRL in the primary cilia may provide a novel mechanism to explain the pathophysiology of Lowe syndrome, but potentially also Dent syndrome. The phenotypes seen in patients with Lowe syndrome, such as congenital cataract and glaucoma, renal dysfunction and neurological defects, all involve highly polarized cell types, such as renal or ocular epithelial cells. Subsequently, it follows that polarity dysregulation in the renal and neurological tissues, which can cause primary cilia signaling defects, could be responsible for the different phenotypes observed in Lowe syndrome (69). We propose that the endocytic defects observed in OCRL knockdown cells may be a consequence of abnormal polarity regulation at the

apical/basolateral membrane (17). Given that OCRL has been shown to localize to the adherens and tight junctions in epithelial cells (8), the breakdown of polarity in these cells may result in the mistrafficking of endocytic vesicles. Interestingly, INPP5B, a paralog of OCRL, was shown to be a positive regulator of cilia length in a large functional genomics screen of modulators of the primary cilia (70). Thus, we propose that inositol phosphatases such as OCRL and INPP5B both regulate ciliary function.

While our *in vitro* studies support a role of OCRL in ciliary function, the lack of phenotype in the murine knockout model can be interpreted in the context of the primary cilia and polarity dysfunction (71). The knockout model of OCRL did not exhibit phenotypes similar to those seen in humans and the *OCRL/INPP5B* double knockout resulted in embryonic lethality, leading to the hypothesis that *INPP5B* may compensate for *OCRL* in the mouse model (70–72). Recently, Bothwell *et al*. (73) developed a murine model of Lowe syndrome that is an *OCRL/INPP5B* double knockout with the human *OCRL* knock-in to rescue the lethal phenotype. In light of our findings, it will be important to examine the function of ciliated cells in the murine models of inositol phosphatase with respect to processes such as eye and kidney development.

Because of OCRL knockout mouse did not exhibit a phenotype, we examined the function of *ocrl* in motile cilia of zebrafish and presented data to show decreased cilia numbers in the KVs in *ocrl* morphant animals. We suggest that OCRL may assist in the recruitment, modification and distribution of critical components of the cilia machinery essential for renewal of the cargo moieties, therefore playing a role in regulating the length of the primary cilium. The maintenance of cilia length can impact the subtle effects of signaling cascades on cellular physiology. OCRL may be added to a growing list of proteins such as IFT components and RPGR that regulate cilia length (33,74,75). Future work is needed to further clarify the role of ciliary proteins in maintaining the polarized distribution of ciliary membrane proteins (76).

During the preparation of this manuscript, Coon *et al*. (77) also showed the localization of OCRL to the cilia and a similar finding of shortened ciliary length in Lowe patient fibroblasts. Our findings agree with their finding; furthermore, using human tissue sections and animal tissue, we showed that OCRL can distribute to the cilia in the absence of RAB8A overexpression and this localization occurs in a number of ciliated cell types, including in ocular cells. In addition, our mutant analysis shows an important role for the 5-phosphatase domain of OCRL in its ciliary localization.

Based on our results, we postulate that the diverse phenotypes present in Lowe syndrome are due to the dysregulation of the primary cilia, with polarity defects in a number of cell types in this genetic disorder. The defects in the protein trafficking in the development and maintenance of the cilia may be the underlying cause for Lowe and Dent syndromes.

MATERIALS AND METHODS

Reagents

Generation and characterization of anti-OCRL antibodies have been described (6); anti-OCRL antibody was affinity purified with beads coated with N-terminal peptide (EPPLPVGAQ-PLATVE(C) (generous gift of Dr Phil Majerus, Washington University, St Louis, MO, USA). Blocking concentration for peptide was 5 mg/ml for immunoblot analysis and 1 mg/ml for immunofluorescence. The γ-tubulin, acetylated α-tubulin, anti-Flag-M2 and EEA1 monoclonal antibodies were obtained from Sigma (St Louis, MO, USA). RAB8A mouse monoclonal antibody was obtained from BD Bioscience (San Diego, CA, USA). Pericentrin, RAB8A rabbit polyclonal antibody was purchased from Abcam (Cambridge, MA, USA). Mouse OCRL monoclonal antibody (OCRL-ms: N166A/26) was obtained from University of California, Davis, NIH/NeuroMabs. Secondary antibodies AlexaFluor 488 and 594-conjugated donkey anti-mouse IgG (1:1000), Cy TM3-conjugated donkey anti-mouse IgG (1:500), horseradish peroxidase-conjugated goat anti-rabbit and anti-mouse IgG were from Jackson ImmunoResearch Laboratories, Inc. (West Grove, PA, USA). IRDye goat anti-mouse and anti-rabbit (680 and 800; 1:20 000) were obtained from Li-cor Bioscience (Lincoln, NB, USA).

DNA constructs

GFP-RAB8A(WT) and GFP-RAB8A(T22N) were previously characterized and obtained from Addgene (47). Flag-OCRL(D422A), Flag-OCRL(D499A), EGFP-OCRL and EGFP-OCRL(delta-RhoGAP) constructs were generous gifts of Dr Alexander Ungewickell (Stanford, CA, USA). Flag-OCRL (F668V) was generated using QuikChangeII kit from Stratagene (Santa Clara, CA, USA). Lentiviral citrine/YFP-OCRL and retroviral RFP-OCRL were generated using Creator (Clontech)-based vectors as described (78).

Human ocular specimens and animal tissue

Human eyes previously removed due to choroidal melanoma but with a normal anterior segment were obtained (University of Michigan IRB no. HUM00034652). Sections were provided by the Histology core service of the University of Michigan, Ann Arbor, MI, USA. For kidney sections, adult female Sprague–Dawley rats (Harlan, Indianapolis, IN, USA) were perfused with 4% paraformaldehyde (PFA) and kidneys were removed and cryosectioned.

Cell culture and transfection

hTERT-RPE1 (American Type Culture Collection) were grown in Dulbecco's Modified Eagle Media (DMEM)/F-12+ GlutaMAX (GIBCO) supplemented with 10% fetal calf serum, penicillin–streptomycin at 37°C in 5% CO_2. Lowe patient fibroblasts (GM1676 and GM3265; Coriell Institute) were cultured in low glucose DMEM 10% fetal calf serum media with penicillin–streptomycin. Lowe 1676 fibroblasts contain a R827X mutation in OCRL gene; Lowe 3265 fibroblasts have markedly decreased OCRL protein levels (Coriell Institute). Primary RPE cells were generous gifts from Dr Monte Del Monte (University of Michigan, Ann Arbor, MI, USA). NPCE cells were generous gifts of Dr Sayoko Moroi (University of Michigan). NHF 588 were generous gifts of Dr Daniel Spandau (Indiana University, Indianapolis, IN, USA).

Transfections were performed using Fugene 6 (Roche) or LipofectAmine 2000 according to the protocol.

Immunofluorescence

Immunofluorescence slides were treated with either PFA for fixation for 10 min at room temperature (RT) followed by permeabilization with 0.5% Triton X-100. For γ-tubulin antibody, methanol/acetone fixation was performed with ice-cold methanol (10 min at −20°C) and permeabilized in ice-cold acetone (10 min at −20°C). Samples were then blocked with phosphate-buffered saline (PBS)/0.5% bovine serum albumin (BSA)/10% normal goat serum (NGS) for 30 min at RT. Cover slips were incubated with the primary antibodies overnight at 4°C followed by secondary antibodies for 45 min at RT, and mounted in ProLong Antifade reagent (Invitrogen). The hTERT-RPE1 cells were synchronized by serum starvation according to previous protocols (48). Cells were imaged on Olympus FV-500 or LEICA SP6 confocal microscope. To evaluate cilia length, Lowe fibroblasts were grown to confluence for 48 h followed by serum deprivation. Cells were then fixed with 4% PFA and cilia growth was analyzed by immunostaining with anti-acetylated α-tubulin antibody from z-stacks (0.25 μm step size) taken with LEICA SP6 confocal microscope or a Zeiss LSM-500 confocal microscope. Ciliary length was measured with NIH Image J software and statistical analysis was performed with SAS. Live imaging was performed using a c-apochromat ×63 oil immersion objective (Zeiss). Cells were grown in 35 mm dishes with embedded cover slips from MatTek at 5% CO_2 at 37°C in an environmental chamber. Live cell images were processed with Zeiss Axiovision 4.8. Confocal images and optical sections were acquired via an Apotome (Zeiss). Time-lapsed movies were taken with CoolSnap camera at indicated time intervals.

Stable cell line generation

RPE cells were transfected with the indicated DNA constructs containing a puromycin selection sequence. Cells were placed in puromycin selection media beginning on day 2 post-transfection. Stable clones were obtained post-selection, cell lysates were made for sodium dodecyl sulfate–polyacrylamide gel electrophoresis (SDS–PAGE) and immunoblot analysis was performed to select for cells expressing indicated protein.

Immunoblot analysis

Cell lysates were subjected to SDS–PAGE followed by immunoblot analysis with the indicated antibodies. Equal amounts of protein were run on 10–12% gel and transferred to nitrocellulose membrane (BioRad). Membranes were blocked in 5% non-fat dried milk in PBS. Primary and secondary antibodies were diluted in concentrations described above. Odyssey Imaging system (Li-Cor Bioscience) was used to analyze the immunoblots.

Knockdown of RAB8A and OCRL1 in cells

RAB8A and control knockdown shRNA lentivirus was obtained from Santa Cruz Biotechnology (Santa Cruz, CA, USA). OCRL siRNA (GGTTCCCTGCCATTTTTCA) was provided by A. Ungewickell and knockdown performed as described (11). The OCRL1 shRNA lentiviral construct was generated using Lentiviral vector pFLRu was gift of Dr Yunfeng Feng, Washington University in St Louis, MO, USA (79). Lentiviral particles were transduced into hTERT-RPE1 cells using as described (79). Knockdown of OCRL1 and RAB8A expression was verified by immunoblotting.

Zebrafish immunohistochemistry and KV cilia measurements

Zebrafish (WT strain: AB *tevbigan*) were raised and maintained at the Laboratory Animal Resource Center of Indiana University. All animal procedures were subject to Institutional animal care and use committee of Indiana University and performed with prior approved protocols. Embryos were fixed overnight at 4°C in 4% PFA and 1% sucrose in PBS. Embyros were dechorionated and washed with PBST for six to eight times 10 min each. After blocking them for 2–4 h with 10% NGS and 0.5% BSA, immunostaining was performed with 1:200 anti-acetylated α-tubulin monoclonal antibody and 1:500 Alexa Fluor 568 goat anti-mouse conjugate separately at 4°C overnight. KV cilia measurements were performed as described (65). Cresyl violet staining was performed as described (53).

Morpolino antisense oligonucleotides knockdown and mRNA rescue in zebrafish

Antisense MOs were designed and purchased from Gene Tools, Inc. Two morpholinos were generated; OCRL ATG initiation codon sequence (OCRL MO1: sequence CGGAAA TCCCAAAT GAAGGTTCCAT) and exon splice donor sequence (OCRL-MO2: sequence ACAAACAGAGAGTCTAC TCACTTGA). A mismatch (MM: sequence ATGCGAAAT CAAGGTTCGATCATCA) morpholino served as a negative control. Morpholinos stocks were dissolved at 1 mM in water: 2 or 4 nl of injection solution (0.25% phenol red) containing 125–500 μM morpholino was injected into fertilized eggs at the one- to two-cell stage using a pressure injector (Pressure System IIe, Toohey Company, Fairfield, NJ, USA). Synthetic mRNA was prepared from linearized human OCRL-pcDNA3.1 DNA with Ambion mMessage mMachine high-yield Capped RNA transcription kit, purified with phenol-chloroform and mRNA was coinjected for rescue experiments. Reverse-transcriptase PCR was performed as described (65).

SUPPLEMENTARY MATERIAL

Supplementary Material is available at *HMG* online.

ACKNOWLEDGEMENTS

We thank Drs Philip Majerus, Stuart Kornfeld, Timothy Corson, Yunfeng Feng, Alexander Ungewickell and Sharon Lee for thoughtful comments during the preparation of the manuscript, Drs Monte Del Monte (University of Michigan) and Sayoko Moroi (University of Michigan) for gifts of RPE cells. We also thank Aaron Muscarella for the care of zebrafish.

Conflict of Interest statement. None declared.

FUNDING

This work was funded by the Pediatric Research Fund from Knights Templar Eye Foundation and a Clinician-Scientist award from American Glaucoma Society to Y.S.; by grants from Foundation Fighting Blindness and Worcester Foundation to H.K; NIH-R01 CA151765 to C.D.W. Funding to pay the Open Access publication charges for this article was provided by Glick Eye Institute, Indiana University.

REFERENCES

1. Bokenkamp, A., Bockenhauer, D., Cheong, H.I., Hoppe, B., Tasic, V., Unwin, R. and Ludwig, M. (2009) Dent-2 disease: a mild variant of Lowe syndrome. *J. Pediatr.*, **155**, 94–99.
2. Hoopes, R.R. Jr, Shrimpton, A.E., Knohl, S.J., Hueber, P., Hoppe, B., Matyus, J., Simckes, A., Tasic, V., Toenshoff, B., Suchy, S.F. *et al.* (2005) Dent Disease with mutations in OCRL1. *Am. J. Hum. Genet.*, **76**, 260–267.
3. Schurman, S.J. and Scheinman, S.J. (2009) Inherited cerebrorenal syndromes. *Nat. Rev. Nephrol.*, **5**, 529–538.
4. McCrea, H.J., Paradise, S., Tomasini, L., Addis, M., Melis, M.A., De Matteis, M.A. and De Camilli, P. (2008) All known patient mutations in the ASH-RhoGAP domains of OCRL affect targeting and APPL1 binding. *Biochem. Biophys. Res. Commun.*, **369**, 493–499.
5. Lowe, M. (2005) Structure and function of the Lowe syndrome protein OCRL1. *Traffic*, **6**, 711–719.
6. Ungewickell, A., Ward, M.E., Ungewickell, E. and Majerus, P.W. (2004) The inositol polyphosphate 5-phosphatase Ocrl associates with endosomes that are partially coated with clathrin. *Proc. Natl Acad. Sci. USA*, **101**, 13501–13506.
7. Hyvola, N., Diao, A., McKenzie, E., Skippen, A., Cockcroft, S. and Lowe, M. (2006) Membrane targeting and activation of the Lowe syndrome protein OCRL1 by rab GTPases. *EMBO J.*, **25**, 3750–3761.
8. Grieve, A.G., Daniels, R.D., Sanchez-Heras, E., Hayes, M.J., Moss, S.E., Matter, K., Lowe, M. and Levine, T.P. (2011) Lowe Syndrome protein OCRL1 supports maturation of polarized epithelial cells. *PLoS ONE*, **6**, e24044.
9. Erdmann, K.S., Mao, Y., McCrea, H.J., Zoncu, R., Lee, S., Paradise, S., Modregger, J., Biemesderfer, D., Toomre, D. and De Camilli, P. (2007) A role of the Lowe syndrome protein OCRL in early steps of the endocytic pathway. *Dev. Cell*, **13**, 377–390.
10. Mao, Y., Balkin, D.M., Zoncu, R., Erdmann, K.S., Tomasini, L., Hu, F., Jin, M.M., Hodsdon, M.E. and De Camilli, P. (2009) A PH domain within OCRL bridges clathrin-mediated membrane trafficking to phosphoinositide metabolism. *EMBO J.*, **28**, 1831–1842.
11. Cui, S., Guerriero, C.J., Szalinski, C.M., Kinlough, C.L., Hughey, R.P. and Weisz, O.A. (2010) OCRL1 function in renal epithelial membrane traffic. *Am. J. Physiol. Renal Physiol.*, **298**, F335–F345.
12. Bohdanowicz, M., Balkin, D.M., De Camilli, P. and Grinstein, S. (2012) Recruitment of OCRL and Inpp5B to phagosomes by Rab5 and APPL1 depletes phosphoinositides and attenuates Akt signaling. *Mol. Biol. Cell*, **23**, 176–187.
13. Zhang, X., Jefferson, A.B., Auethavekiat, V. and Majerus, P.W. (1995) The protein deficient in Lowe syndrome is a phosphatidylinositol-4,5-bisphosphate 5-phosphatase. *Proc. Natl Acad. Sci. USA*, **92**, 4853–4856.
14. Dambournet, D., Machicoane, M., Chesneau, L., Sachse, M., Rocancourt, M., El Marjou, A., Formstecher, E., Salomon, R., Goud, B. and Echard, A. (2011) Rab35 GTPase and OCRL phosphatase remodel lipids and F-actin for successful cytokinesis. *Nat. Cell Biol.*, **13**, 981–988.
15. Choudhury, R., Noakes, C.J., McKenzie, E., Kox, C. and Lowe, M. (2009) Differential clathrin binding and subcellular localization of OCRL1 splice isoforms. *J. Biol. Chem.*, **284**, 9965–9973.
16. Choudhury, R., Diao, A., Zhang, F., Eisenberg, E., Saint-Pol, A., Williams, C., Konstantakopoulos, A., Lucocq, J., Johannes, L., Rabouille, C. *et al.* (2005) Lowe syndrome protein OCRL1 interacts with clathrin and regulates protein trafficking between endosomes and the trans-Golgi network. *Mol. Biol. Cell*, **16**, 3467–3479.
17. Vicinanza, M., Di Campli, A., Polishchuk, E., Santoro, M., Di Tullio, G., Godi, A., Levtchenko, E., De Leo, M.G., Polishchuk, R., Sandoval, L. *et al.* (2011) OCRL controls trafficking through early endosomes via PtdIns4,5P(2)-dependent regulation of endosomal actin. *EMBO J.*, **24**, 4970–4985.
18. Noakes, C.J., Lee, G. and Lowe, M. (2011) The PH domain proteins IPIP27A and B link OCRL1 to receptor recycling in the endocytic pathway. *Mol. Biol. Cell*, **22**, 606–623.
19. Swan, L.E., Tomasini, L., Pirruccello, M., Lunardi, J. and De Camilli, P. (2010) Two closely related endocytic proteins that share a common OCRL-binding motif with APPL1. *Proc. Natl Acad. Sci. USA*, **107**, 3511–3516.
20. Hou, X., Hagemann, N., Schoebel, S., Blankenfeldt, W., Goody, R.S., Erdmann, K.S. and Itzen, A. (2011) A structural basis for Lowe syndrome caused by mutations in the Rab-binding domain of OCRL1. *EMBO J.*, **30**, 1659–1670.
21. Lichter-Konecki, U., Farber, L.W., Cronin, J.S., Suchy, S.F. and Nussbaum, R.L. (2006) The effect of missense mutations in the RhoGAP-homology domain on ocrl1 function. *Mol. Genet. Metab.*, **89**, 121–128.
22. Suchy, S.F. and Nussbaum, R.L. (2002) The deficiency of PIP2 5-phosphatase in Lowe syndrome affects actin polymerization. *Am. J. Hum. Genet.*, **71**, 1420–1427.
23. Coon, B.G., Mukherjee, D., Hanna, C.B., Riese, D.J. 2nd, Lowe, M. and Aguilar, R.C. (2009) Lowe syndrome patient fibroblasts display Ocrl1-specific cell migration defects that cannot be rescued by the homologous Inpp5b phosphatase. *Hum. Mol. Genet.*, **18**, 4478–4491.
24. Liem, K.F. Jr, He, M., Ocbina, P.J. and Anderson, K.V. (2009) Mouse Kif7/Costal2 is a cilia-associated protein that regulates Sonic hedgehog signaling. *Proc. Natl Acad. Sci. USA*, **106**, 13377–13382.
25. Pugacheva, E.N., Jablonski, S.A., Hartman, T.R., Henske, E.P. and Golemis, E.A. (2007) HEF1-dependent Aurora A activation induces disassembly of the primary cilium. *Cell*, **129**, 1351–1363.
26. Schneider, L., Clement, C.A., Teilmann, S.C., Pazour, G.J., Hoffmann, E.K., Satir, P. and Christensen, S.T. (2005) PDGFRalphaalpha signaling is regulated through the primary cilium in fibroblasts. *Curr. Biol.*, **15**, 1861–1866.
27. Wong, S.Y., Seol, A.D., So, P.L., Ermilov, A.N., Bichakjian, C.K., Epstein, E.H. Jr, Dlugosz, A.A. and Reiter, J.F. (2009) Primary cilia can both mediate and suppress Hedgehog pathway-dependent tumorigenesis. *Nat. Med.*, **15**, 1055–1061.
28. Graser, S., Stierhof, Y.D., Lavoie, S.B., Gassner, O.S., Lamla, S., Le Clech, M. and Nigg, E.A. (2007) Cep164, a novel centriole appendage protein required for primary cilium formation. *J. Cell Biol.*, **179**, 321–330.
29. McKean, P.G., Baines, A., Vaughan, S. and Gull, K. (2003) Gamma-tubulin functions in the nucleation of a discrete subset of microtubules in the eukaryoticflagellum. *Curr. Biol.*, **13**, 598–602.
30. Piperno, G., LeDizet, M. and Chang, X.J. (1987) Microtubules containing acetylated alpha-tubulin in mammalian cells in culture. *J. Cell Biol.*, **104**, 289–302.
31. Jackson, P.K. (2011) Do cilia put brakes on the cell cycle? *Nat. Cell Biol.*, **13**, 340–342.
32. Pearson, C.G., Culver, B.P. and Winey, M. (2007) Centrioles want to move out and make cilia. *Dev. Cell*, **13**, 319–321.
33. Ishikawa, H. and Marshall, W.F. (2011) Ciliogenesis: building the cell's antenna. *Nat. Rev. Mol. Cell Biol.*, **12**, 222–234.
34. Praetorius, H.A. and Spring, K.R. (2005) A physiological view of the primary cilium. *Annu. Rev. Physiol.*, **67**, 515–529.

35. Scholey, J.M. (2003) Intraflagellar transport. *Annu. Rev. Cell Dev. Biol.*, **19**, 423–443.
36. Sedmak, T. and Wolfrum, U. (2010) Intraflagellar transport molecules in ciliary and nonciliary cells of the retina. *J. Cell Biol.*, **189**, 171–186.
37. Sharma, N., Kosan, Z.A., Stallworth, J.E., Berbari, N.F. and Yoder, B.K. (2011) Soluble levels of cytosolic tubulin regulate ciliary length control. *Mol. Biol. Cell*, **22**, 806–816.
38. den Hollander, A.I., Koenekoop, R.K., Mohamed, M.D., Arts, H.H., Boldt, K., Towns, K.V., Sedmak, T., Beer, M., Nagel-Wolfrum, K., McKibbin, M. *et al.* (2007) Mutations in LCA5, encoding the ciliary protein lebercilin, cause Leber congenital amaurosis. *Nat. Genet.*, **39**, 889–895.
39. Hildebrandt, F., Benzing, T. and Katsanis, N. (2011) Ciliopathies. *N. Engl. J. Med.*, **364**, 1533–1543.
40. Novarino, G., Akizu, N. and Gleeson, J.G. (2011) Modeling human disease in humans: the ciliopathies. *Cell*, **147**, 70–79.
41. Kisseleva, M.V., Wilson, M.P. and Majerus, P.W. (2000) The isolation and characterization of a cDNA encoding phospholipid-specific inositol polyphosphate 5-phosphatase. *J. Biol. Chem.*, **275**, 20110–20116.
42. Bielas, S.L., Silhavy, J.L., Brancati, F., Kisseleva, M.V., Al-Gazali, L., Sztriha, L., Bayoumi, R.A., Zaki, M.S., Abdel-Aleem, A., Rosti, R.O. *et al.* (2009) Mutations in INPP5E, encoding inositol polyphosphate-5-phosphatase E, link phosphatidyl inositol signaling to the ciliopathies. *Nat. Genet.*, **41**, 1032–1036.
43. Walton, D.S., Katsavounidou, G. and Lowe, C.U. (2005) Glaucoma with the oculocerebrorenal syndrome of Lowe. *J. Glaucoma*, **14**, 181–185.
44. Ohnishi, Y. and Tanaka, M. (1980) Cilia in the ciliary epithelium. *Albrecht Von Graefes Arch. Klin. Exp. Ophthalmol.*, **213**, 161–167.
45. Piperno, G. and Fuller, M.T. (1985) Monoclonal antibodies specific for an acetylated form of alpha-tubulin recognize the antigen in cilia and flagella from a variety of organisms. *J. Cell Biol.*, **101**, 2085–2094.
46. Walter, R.J., Malech, H.L. and Oliver, J.M. (1983) Cell motility and microtubules in cultured fibroblasts from patients with Kartagener syndrome. *Cell Motil.*, **3**, 185–197.
47. Nachury, M.V., Loktev, A.V., Zhang, Q., Westlake, C.J., Peranen, J., Merdes, A., Slusarski, D.C., Scheller, R.H., Bazan, J.F., Sheffield, V.C. *et al.* (2007) A core complex of BBS proteins cooperates with the GTPase Rab8 to promote ciliary membrane biogenesis. *Cell*, **129**, 1201–1213.
48. Murga-Zamalloa, C.A., Atkins, S.J., Peranen, J., Swaroop, A. and Khanna, H. (2010) Interaction of retinitis pigmentosa GTPase regulator (RPGR) with RAB8A GTPase: implications for cilia dysfunction and photoreceptor degeneration. *Hum. Mol. Genet.*, **19**, 3591–3598.
49. Westlake, C.J., Baye, L.M., Nachury, M.V., Wright, K.J., Ervin, K.E., Phu, L., Chalouni, C., Beck, J.S., Kirkpatrick, D.S., Slusarski, D.C. *et al.* (2011) Primary cilia membrane assembly is initiated by Rab11 and transport protein particle II (TRAPPII) complex-dependent trafficking of Rabin8 to the centrosome. *Proc. Natl Acad. Sci. USA*, **108**, 2759–2764.
50. Yoshimura, S., Egerer, J., Fuchs, E., Haas, A.K. and Barr, F.A. (2007) Functional dissection of Rab GTPases involved in primary cilium formation. *J. Cell Biol.*, **178**, 363–369.
51. Ooms, L.M., Horan, K.A., Rahman, P., Seaton, G., Gurung, R., Kethesparan, D.S. and Mitchell, C.A. (2009) The role of the inositol polyphosphate 5-phosphatases in cellular function and human disease. *Biochem. J.*, **419**, 29–49.
52. Chakarova, C.F., Khanna, H., Shah, A.Z., Patil, S.B., Sedmak, T., Murga-Zamalloa, C.A., Papaioannou, M.G., Nagel-Wolfrum, K., Lopez, I., Munro, P. *et al.* (2011) TOPORS, implicated in retinal degeneration, is a cilia-centrosomal protein. *Hum. Mol. Genet.*, **20**, 975–987.
53. Hurd, T., Zhou, W., Jenkins, P., Liu, C.J., Swaroop, A., Khanna, H., Martens, J., Hildebrandt, F. and Margolis, B. (2010) The retinitis pigmentosa protein RP2 interacts with polycystin 2 and regulates cilia-mediated vertebrate development. *Hum. Mol. Genet.*, **19**, 4330–4344.
54. Hirokawa, N., Tanaka, Y., Okada, Y. and Takeda, S. (2006) Nodal flow and the generation of left-right asymmetry. *Cell*, **125**, 33–45.
55. Wright, A.F., Chakarova, C.F., Abd El-Aziz, M.M. and Bhattacharya, S.S. (2010) Photoreceptor degeneration: genetic and mechanistic dissection of a complex trait. *Nat. Rev. Genet.*, **11**, 273–284.
56. Nachury, M.V., Seeley, E.S. and Jin, H. (2010) Trafficking to the ciliary membrane: how to get across the periciliary diffusion barrier? *Annu. Rev. Cell. Dev. Biol.*, **26**, 59–87.
57. Friedman, J.S., Chang, B., Krauth, D.S., Lopez, I., Waseem, N.H., Hurd, R.E., Feathers, K.L., Branham, K.E., Shaw, M., Thomas, G.E. *et al.* (2010) Loss of lysophosphatidylcholine acyltransferase 1 leads to photoreceptor degeneration in rd11 mice. *Proc. Natl Acad. Sci. USA*, **107**, 15523–15528.
58. Otto, E.A., Hurd, T.W., Airik, R., Chaki, M., Zhou, W., Stoetzel, C., Patil, S.B., Levy, S., Ghosh, A.K., Murga-Zamalloa, C.A. *et al.* (2010) Candidate exome capture identifies mutation of SDCCAG8 as the cause of a retinal-renal ciliopathy. *Nat. Genet.*, **42**, 840–850.
59. Richardson, G.P., de Monvel, J.B. and Petit, C. (2011) How the genetics of deafness illuminates auditory physiology. *Annu. Rev. Physiol.*, **73**, 311–334.
60. Khanna, H., Davis, E.E., Murga-Zamalloa, C.A., Estrada-Cuzcano, A., Lopez, I., den Hollander, A.I., Zonneveld, M.N., Othman, M.I., Waseem, N., Chakarova, C.F. *et al.* (2009) A common allele in RPGRIP1L is a modifier of retinal degeneration in ciliopathies. *Nat. Genet.*, **41**, 739–745.
61. Louie, C.M. and Gleeson, J.G. (2005) Genetic basis of Joubert syndrome and related disorders of cerebellar development. *Hum. Mol. Genet.*, **14**(Spec No. 2), R235–R242.
62. Lancaster, M.A., Gopal, D.J., Kim, J., Saleem, S.N., Silhavy, J.L., Louie, C.M., Thacker, B.E., Williams, Y., Zaki, M.S. and Gleeson, J.G. (2011) Defective Wnt-dependent cerebellar midline fusion in a mouse model of Joubert syndrome. *Nat. Med.*, **17**, 726–731.
63. Zhang, X., Hartz, P.A., Philip, E., Racusen, L.C. and Majerus, P.W. (1998) Cell lines from kidney proximal tubules of a patient with Lowe syndrome lack OCRL inositol polyphosphate 5-phosphatase and accumulate phosphatidylinositol 4,5-bisphosphate. *J. Biol. Chem.*, **273**, 1574–1582.
64. Wu, T.C. and Grotta, J.C. (2010) Stroke treatment and prevention: five new things. *Neurology*, **75**, S16–S21.
65. Murga-Zamalloa, C.A., Ghosh, A.K., Patil, S.B., Reed, N.A., Chan, L.S., Davuluri, S., Peranen, J., Hurd, T.W., Rachel, R.A. and Khanna, H. (2011) Accumulation of the Raf-1 kinase inhibitory protein (Rkip) is associated with Cep290-mediated photoreceptor degeneration in ciliopathies. *J. Biol. Chem.*, **286**, 28276–28286.
66. Lewis, R.A., Nussbaum, R.L. and Brewer, E.D. (1993–2001) Lowe syndrome. *GeneReviews*, July 24.
67. Jacoby, M., Cox, J.J., Gayral, S., Hampshire, D.J., Ayub, M., Blockmans, M., Pernot, E., Kisseleva, M.V., Compere, P., Schiffmann, S.N. *et al.* (2009) INPP5E mutations cause primary cilium signaling defects, ciliary instability and ciliopathies in human and mouse. *Nat. Genet.*, **41**, 1027–1031.
68. Fukuda, M., Kanno, E., Ishibashi, K. and Itoh, T. (2008) Large scale screening for novel rab effectors reveals unexpected broad Rab binding specificity. *Mol. Cell Proteomics*, **7**, 1031–1042.
69. Koo, J.H., Gill, S., Pannell, L.K., Menco, B.P., Margolis, J.W. and Margolis, F.L. (2004) The interaction of Bex and OMP reveals a dimer of OMP with a short half-life. *J. Neurochem.*, **90**, 102–116.
70. Kim, J., Lee, J.E., Heynen-Genel, S., Suyama, E., Ono, K., Lee, K., Ideker, T., Aza-Blanc, P. and Gleeson, J.G. (2010) Functional genomic screen for modulators of ciliogenesis and cilium length. *Nature*, **464**, 1048–1051.
71. Janne, P.A., Suchy, S.F., Bernard, D., MacDonald, M., Crawley, J., Grinberg, A., Wynshaw-Boris, A., Westphal, H. and Nussbaum, R.L. (1998) Functional overlap between murine Inpp5b and Ocrl1 may explain why deficiency of the murine ortholog for OCRL1 does not cause Lowe syndrome in mice. *J. Clin. Invest.*, **101**, 2042–2053.
72. Hellsten, E., Bernard, D.J., Owens, J.W., Eckhaus, M., Suchy, S.F. and Nussbaum, R.L. (2002) Sertoli cell vacuolization and abnormal germ cell adhesion in mice deficient in an inositol polyphosphate 5-phosphatase. *Biol. Reprod.*, **66**, 1522–1530.
73. Bothwell, S.P., Chan, E., Bernardini, I.M., Kuo, Y.M., Gahl, W.A. and Nussbaum, R.L. (2011) Mouse model for Lowe syndrome/Dent Disease 2 renal tubulopathy. *J. Am. Soc. Nephrol.*, **22**, 443–448.
74. Engel, B.D., Ludington, W.B. and Marshall, W.F. (2009) Intraflagellar transport particle size scales inversely with flagellar length: revisiting the balance-point length control model. *J. Cell Biol.*, **187**, 81–89.
75. Yoder, B.K. (2006) More than just the postal service: novel roles for IFT proteins in signal transduction. *Dev. Cell*, **10**, 541–542.
76. Ponting, C.P. (2006) A novel domain suggests a ciliary function for ASPM, a brain size determining gene. *Bioinformatics*, **22**, 1031–1035.
77. Coon, B.G., Hernandez, V., Madhivanan, K., Mukherjee, D., Hanna, C.B., Barinaga-Rementeria Ramirez, I., Lowe, M., Beales, P.L. and Aguilar, R.C. (2012) The Lowe syndrome protein OCRL1 is involved in primary cilia assembly. *Hum. Mol. Genet.*, **21**, 1835–1847.

78. Colwill, K., Wells, C.D., Elder, K., Goudreault, M., Hersi, K., Kulkarni, S., Hardy, W.R., Pawson, T. and Morin, G.B. (2006) Modification of the Creator recombination system for proteomics applications—improved expression by addition of splice sites. *BMC Biotechnol.*, **6**, 13.

79. Feng, Y., Nie, L., Thakur, M.D., Su, Q., Chi, Z., Zhao, Y. and Longmore, G.D. (2010) A multifunctional lentiviral-based gene knockdown with concurrent rescue that controls for off-target effects of RNAi. *Genomics Proteomics Bioinformatics*, **8**, 238–245.